Reduced-Order Modeling of Composite Floor Slabs in Fire. I: Heat-Transfer Analysis

Jian Jiang[1]; Joseph A. Main, M.ASCE[2]; Jonathan M. Weigand, A.M.ASCE[3]; and Fahim Sadek, M.ASCE[4]

Abstract: This paper presents a reduced-order numerical modeling approach for the analysis of heat transfer in composite floor slabs with profiled steel decking exposed to fire effects. This approach represents the thick and thin portions of a composite slab with alternating strips of shell elements, using a layered thick-shell formulation that accounts for both in-plane and through-thickness heat transfer. To account for the tapered profile of the ribs, layered shell elements representing the thick portion of the slab adopt a linear reduction in the density of concrete within the depth in the rib. The specific heat of concrete in the rib is also proportionally reduced to indirectly consider the heat input through the web of the decking, because the reduced-order model considers thermal loading only on the upper and lower flanges of the decking. The optimal ratio of modified and actual specific heat of concrete in the rib is determined, depending on the ratio of the height of the upper continuous portion to the height of the rib. The reduced-order modeling approach is validated against experimental results. **DOI: 10.1061/(ASCE)ST.1943-541X.0002650.** *© 2020 American Society of Civil Engineers.*

Author keywords: Composite slab; Heat transfer analysis; Reduced-order model; Shell element; Steel decking.

Introduction

Composite slabs consisting of concrete topping on profiled steel decking are widely used as floor systems in modern steel-framed buildings. Typically, the concrete is lightly reinforced using welded-wire mesh to control temperature and shrinkage cracks. Reinforcing bars are sometimes placed in the concrete topping or within the ribs of the decking. Composite slabs are typically attached to primary steel beams at the perimeter and sometimes supported by secondary beams in the interior, both by means of shear studs to develop composite action. The decking also acts as reinforcement, which lowers the center of reinforcement of the slab, and thus composite slabs require considerably less concrete than conventional reinforced-concrete slabs. Another advantage of composite slabs over conventional slabs is reduced construction time, given that the decking also serves as permanent formwork. The use of composite slabs in buildings has been common in North America for many years and has experienced a rapid increase in Europe since the 1980s. However, when composite slabs are exposed to fire effects, the presence of the ribs results in thermal and structural responses that are more complex than those for a flat slab, presenting challenges in numerical analysis and practical design.

Analyzing the response of composite slabs to fire-induced thermal loading requires both heat transfer analysis and structural analysis. Both thermal and structural analyses of composite slabs present their own unique challenges, and different types of models are typically used, which introduces an additional challenge of transferring analysis results between models with different element types and potentially different mesh resolutions. A key objective of this study is to develop a reduced-order modeling approach for thermal analysis that is also suitable for structural analysis. Reduced-order models that could be used for both thermal and structural analysis would facilitate evaluation of the response of structural system under various fire scenarios, including realistic thermal loading obtained from computational simulations of fire dynamics.

Numerical analysis of heat transfer in composite slabs typically uses a detailed finite-element modeling approach, with solid elements for the concrete slab and shell elements for the steel decking (e.g., Hamerlinck et al. 1990; Lamont et al. 2004; Guo 2012; Pantousa and Mistakidis 2013; Jiang et al. 2017). As is further discussed in the companion paper (Jiang et al., forthcoming), structural analysis of fire effects on composite slabs commonly uses shell element formulations (e.g., Huang et al. 2000; Izzuddin et al. 2004), grillage-type beam element models (e.g., Elghazouli and Izzuddin 2000; Sanad et al. 2000a, b), or hybrid approaches with both beam and shell elements (e.g., Lim et al. 2004). The grillage modeling approach with beam elements is clearly unsuitable for thermal analysis, because of the inadequacy of the 1D elements to represent in-plane and through-thickness heat transfer in the slab. Shell-element modeling approaches typically use a constant shell thickness, which is unsuitable for thermal analysis because it fails to capture the thermal shielding effect of the ribs. This effect results in curved isotherms in the floor slab, affecting both the structural response and the thermal insulation provided by the slab. Because of the inadequacy of 1D elements to capture the complexities of heat transfer in composite floor slabs, hybrid approaches that use both shell and beam elements are also unsuitable for thermal analysis.

This paper proposes a reduced-order modeling approach consisting of alternating strips of layered shell elements to represent

[1]Research Structural Engineer, Engineering Laboratory, National Institute of Standards and Technology, 100 Bureau Dr., Mail Stop 8611, Gaithersburg, MD 20899-8611.

[2]Research Structural Engineer, Engineering Laboratory, National Institute of Standards and Technology, 100 Bureau Dr., Mail Stop 8611, Gaithersburg, MD 20899-8611.

[3]Research Structural Engineer, Engineering Laboratory, National Institute of Standards and Technology, 100 Bureau Dr., Mail Stop 8611, Gaithersburg, MD 20899-8611 (corresponding author). ORCID: https://orcid.org/0000-0002-6938-6197. Email: jonathan.weigand@nist.gov; jweigand@uw.edu

[4]Research Structural Engineer, Engineering Laboratory, National Institute of Standards and Technology, 100 Bureau Dr., Mail Stop 8611, Gaithersburg, MD 20899-8611.

Note. This manuscript was submitted on April 24, 2019; approved on November 18, 2019; published online on March 19, 2020. Discussion period open until August 19, 2020; separate discussions must be submitted for individual papers. This paper is part of the ***Journal of Structural Engineering***, © ASCE, ISSN 0733-9445.

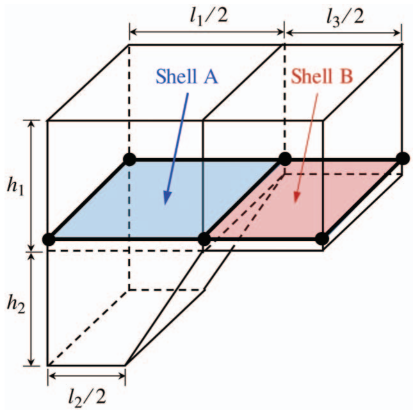

Fig. 1. (Color) Representation of composite slab using alternating strips of shell elements.

the thick and thin portions of the composite slab, building on approaches previously used for structural analysis by Kwasniewski (2010) and Main (2014). This approach is well-suited both for heat transfer analysis, as discussed in this paper, and for structural analysis, as discussed in the companion paper (Jiang et al., forthcoming). Both types of analysis require approximations to account for the profile of the decking and the ribs. In the reduced-order modeling for heat transfer analysis, as presented in this paper, a "dummy material" with high through-thickness thermal conductivity and low specific heat is used to represent the voids between the ribs, and a linear reduction in the density of concrete in the ribs is used to represent the tapered profile of the ribs. Modifications in the specific heat of concrete in the rib are incorporated to indirectly account for heat input through the web of the decking, because thermal loading can only be directly applied to the upper and lower flanges of the decking in the reduced-order modeling approach. Comparisons with temperature histories from detailed finite-element models were used to determine the optimal modification of the specific heat as a function of the slab dimensions. Finally, validation of the reduced-order modeling approach is presented through comparisons with experimental measurements.

Reduced-Order Modeling Approach

Use of shell elements in the reduced-order modeling approach enables large-scale structural systems to be analyzed much more efficiently than detailed approaches using solid elements. The proposed reduced-order modeling approach uses a layered composite shell formulation, in which a distinct structural material, thermal material, and thickness can be specified for each layer (*PART_COMPOSITE in LS-DYNA). This allows distinct layers to be specified for the steel decking and the reinforcement, with multiple layers representing concrete specified through the thickness of the slab. A thick thermal shell formulation is used, which allows for both in-plane and through-thickess heat conduction, with thermal gradients through the thickness of each layer. The geometry of the slab is captured using alternating strips of shell elements to represent the thick and thin portions of the composite slab, as illustrated in Fig. 1. For the periodic slab configuration, only two shell elements are needed in the reduced-order modeling approach, i.e., Shell A for the thick portion of the slab and Shell B for the thin portion (Fig. 1).

Fig. 2 illustrates the layers of material used to represent the thick part of the slab (Shell A) and the thin part of the slab (Shell B) in the composite shell formulation. Based on mesh sensitivity analyses reported by Jiang et al. (2017), it was found that sufficient accuracy could be achieved by using four layers in the composite shell to represent the upper portion of the concrete slab and using an additional four layers to represent the concrete in the rib (Fig. 2). An additional layer in Shell A was used to represent the lower flange of the steel decking, and an additional layer in Shell B was used to represent the upper flange of the decking. Fig. 2 illustrates the following two aspects of the reduced-order modeling approach, which are discussed in the subsequent subsections:

1. Reduction of the concrete density in the ribs to represent the tapered profile (section "Reduction of Concrete Density in Ribs to Represent Tapered Profile")
2. Use of a "dummy material" to represent the voids between the ribs (section "'Dummy Material' to Represent Voids Between Ribs")

Reduction of Concrete Density in Ribs to Represent Tapered Profile

As observed in parametric studies on composite slab geometry by Jiang et al. (2017), the mass of concrete in the rib can significantly influence the temperatures in the slab above the rib. Therefore, accounting for the tapered profile of the rib is important in order to accurately represent the total mass of concrete in the rib, as well as its distribution. In the reduced-order modeling approach, the profile of the rib cannot be directly specified by using different widths for

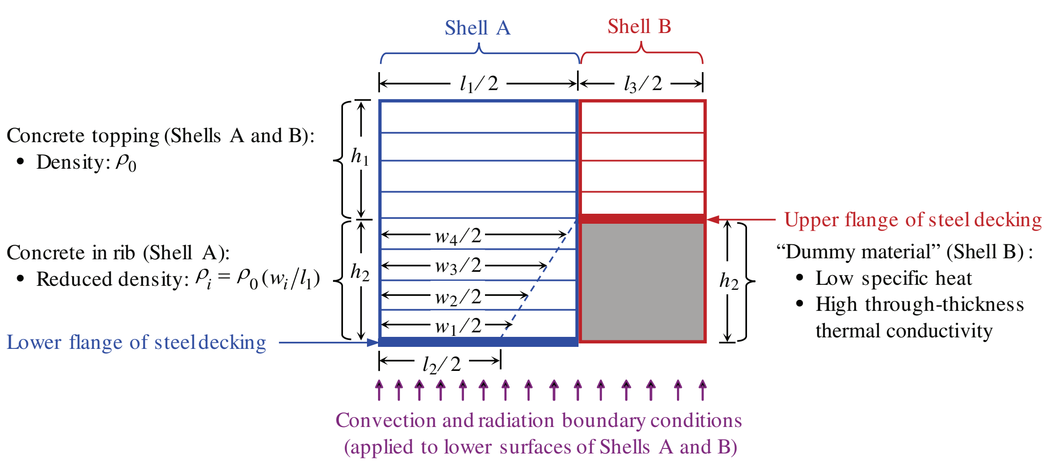

Fig. 2. (Color) Layered-shell representation of thick and thin portions of composite slab.

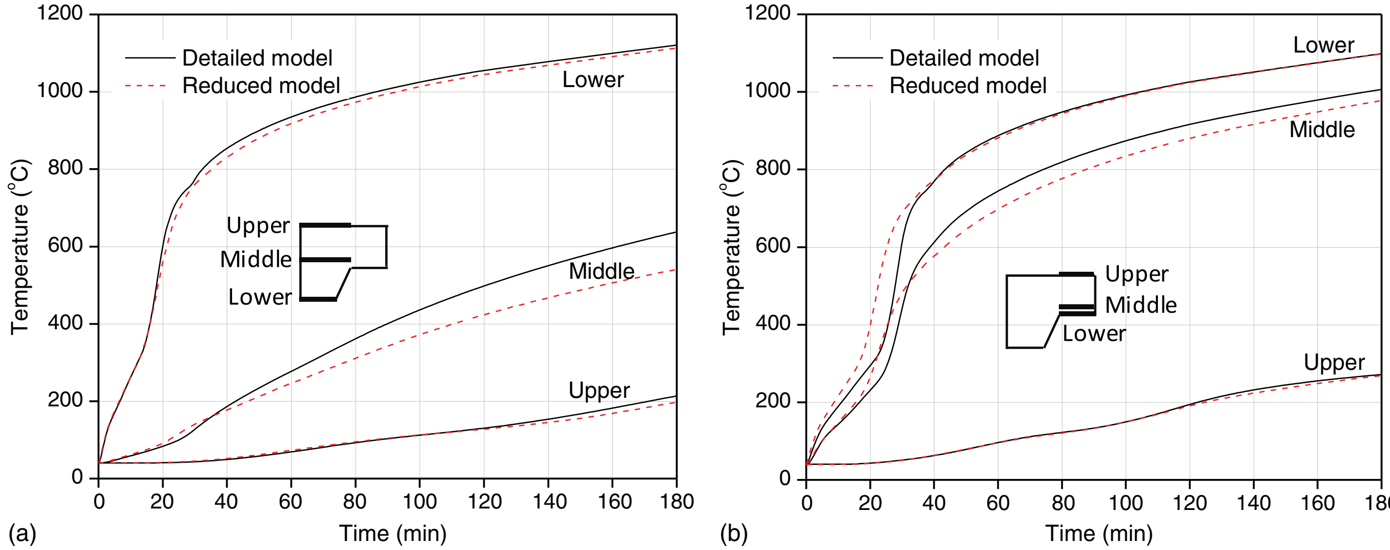

Fig. 3. (Color) Comparison of layer-averaged temperature histories from the detailed model and reduced-order model: (a) thick portion of slab; and (b) thin portion of slab.

different layers, because the composite shell formulation assumes constant in-plane dimensions for all layers. Instead, the profile of the rib is accounted for in Shell A by reducing the density of concrete in the rib to accurately represent the mass of concrete in each layer. As illustrated in Fig. 2, the reduced concrete density for the ith layer of the rib, ρ_i, is calculated based on the ratio of the average rib width for that layer, w_i, to the total width at the top of the rib, l_1, as $\rho_i = \rho_0 \times (w_i/l_1)$, where ρ_0 is the concrete density.

"Dummy Material" to Represent Voids between Ribs

In modeling the thin portion of the slab (Shell B), a dummy material with low specific heat and high through-thickness thermal conductivity is used to represent the voids between the ribs, with a height h_2 equal to the rib height, as illustrated in Fig. 2. The key reason for incorporating the dummy material into Shell B is to allow Shell A and Shell B to have the same thickness, which is required for proper modeling of in-plane heat conduction between corresponding layers of adjoining shell elements. Using the same thickness also allows the nodes of Shell A and Shell B to be defined in a common plane, which in this study was at midheight of the thick portion of the slab (Fig. 1). In a coupled thermal-structural analysis, a structural material model with negligible stiffness and strength would also be assigned to the dummy material, as was done in Main (2014), although this study considers thermal analysis only. Radiation and convection boundary conditions are applied at the fictitious lower surface of Shell B. A high through-thickness thermal conductivity for the dummy material, along with low specific heat [values of 100 $\mathrm{W/(m \cdot K)}$ and 1 $\mathrm{J/(kg \cdot K)}$, respectively, were used in this study], ensure an essentially equivalent temperature at the top of the dummy material, thus providing appropriate thermal boundary conditions for the upper flange of the steel decking. Radiation and convection boundary conditions are also applied to the bottom surface of Shell A to model the heat input through the lower flange of the steel decking.

Heat input through the web of the decking cannot be directly modeled in the layered composite shell formulation, because the web of the decking is not included in the model. However, the essentially uniform temperature through the depth of the dummy material (which is generally quite close to the gas temperature, as a result of the radiation and convection boundary conditions) does result in heat flux into the cooler adjoining layers in the rib of Shell A, thus partially accounting for heat input through the web of the decking.

Comparison with Detailed Model Results for Baseline Slab Configuration

Fig. 3 shows a comparison of temperature histories computed using the reduced-order modeling approach with corresponding temperature histories computed using a detailed modeling approach described by Jiang et al. (2017), in which the lightweight concrete slab was modeled using solid elements and the steel decking was modeled using shell elements. The comparison in Fig. 3 corresponds to the baseline composite slab geometry shown in Fig. 4, which incorporates Vulcraft 3VLI decking with a thickness of 0.9 mm. The same thermal boundary conditions (convection and radiation) were used in the reduced-order model as in the detailed model, except that thermal loading on the web of the decking could only be directly included in the detailed modeling approach, not in the reduced-order modeling approach, as noted above. The gas temperature history was determined from the ISO 834 standard fire curve (ISO 2014) and the convective heat transfer coefficient was taken as 25 $\mathrm{W/(m^2 \cdot K)}$ for the lower flange of the decking, with a reduced value of 15 $\mathrm{W/(m^2 \cdot K)}$ for the upper flange of the decking and the web (in the detailed model), to consider the shielding effect of the ribs. The temperature-dependent emissivity proposed by Jiang et al. (2017) was used for the galvanized decking, with emissivities of 0.1 and 0.7 at temperatures below 400°C and above 800°C, respectively, and a linear variation between

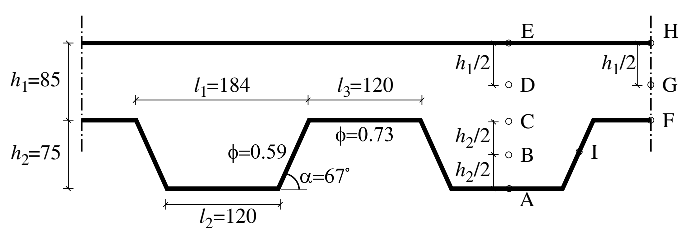

Fig. 4. Typical composite slab configuration with Vulcraft 3VLI decking (dimensions in millimeters).

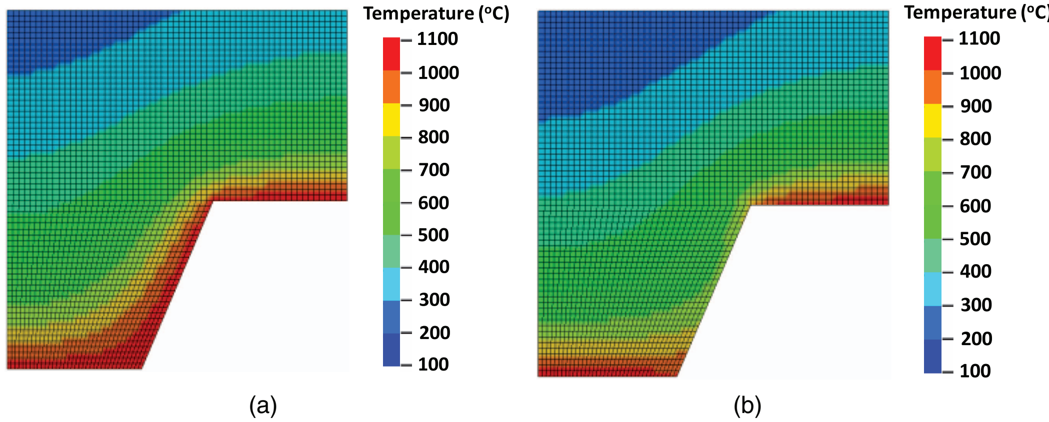

Fig. 5. (Color) Comparison of temperature contours from detailed models at 180 min: (a) thermal loading on all decking surfaces; and (b) no thermal loading on web.

0.1 and 0.7 for temperatures between 400°C and 800°C. A constant emissivity of 0.7 was used for the concrete at the unexposed surface. The thermal properties for lightweight concrete, including the specific heat, were taken from Eurocode 4 (CEN 2005) based on an assumed moisture content of 5%. In the Eurocode 4 model, the specific heat is increased for temperatures between 100°C and 200°C to account for the evaporation of free moisture, with a peak value of the specific heat at 115°C.

The temperature histories presented in Fig. 3 correspond to layer-averaged temperatures. Shell-element temperatures at the lower, middle, and upper surfaces are presented from the reduced-order model, and layer-averaged temperatures from the detailed model were calculated at consistent elevations. The high through-thickness thermal conductivity of the dummy material ensured that the temperature at the fictitious lower surface of Shell B was virtually equivalent to the temperature in the upper flange of the steel decking. For this reason, the upper flange of the steel decking is labeled as the lower surface in Fig. 3(b). The temperature deviations between the reduced-order and detailed models in Fig. 3 resulted from approximations inherent in the layered composite shell formulation, which underestimated the heat input through the web of the decking. This resulted in delayed heating just above the rib [middle surface in Fig. 3(a)], where the reduced-order model underestimated the temperature by about 16% at the end of the analysis. Better agreement was observed for the temperature histories at other locations.

Fig. 5(a) shows computed temperature contours from the detailed model after 180 min of heating, and Fig. 5(b) shows corresponding temperature contours from a detailed model in which thermal loading was applied only to the upper and lower flanges of the decking, not to the web. Comparison of these temperature contours shows that the influence of heat input through the web resulted in noticeably increased temperatures at the top of the rib in Fig. 5(a) relative to Fig. 5(b). This corresponds to the middle surface of the thick portion of the slab, where the largest discrepancy was observed between the detailed and reduced-order models in Fig. 3(a), as a result of underestimating the heat input through the web of the decking. The following section presents an approach that was developed to better capture the heat input through the web in the reduced-order modeling approach.

Modification of Specific Heat for Concrete in the Ribs

It is evident in Fig. 5 that the heat input through the web of the decking has a significant influence on the temperature distribution within the slab, especially near the top of the rib. To reduce the discrepancies in temperatures from the reduced-order model at this location [Fig. 3(a), middle surface], it is necessary to better capture the heat input through the web of the decking. Several methods to accomplish this were considered, one of which was to modify the thermal boundary conditions in order to provide additional heat input. However, the most effective approach was found to be through modification of the specific heat of the concrete in the rib. An empirical scale factor was thus introduced for the specific heat to account for the approximations inherent in the proposed approach. The scaled specific heat, denoted c_p', was used for the concrete in the rib, while the actual specific heat, c_p, was used for the rest of the concrete in the slab. A reduction in the specific heat indirectly accounts for additional heat input through the web, since the reduced specific heat increases the thermal diffusivity, thus increasing the rate of heat flow through the rib. This approach allowed for improved accuracy in the temperature above the rib, with minimal effect on the temperatures at other locations in the slab, where the discrepancies in Fig. 3 were already quite small.

The optimal value of c_p'/c_p was determined by minimizing the root-mean-square (RMS) deviation between the temperature histories from the reduced-order and detailed models, defined as follows:

$$T_{\mathrm{RMSD}} = \sqrt{\frac{\sum_{i=1}^{n} (T_{\mathrm{R}}(t_i) - T_{\mathrm{D}}(t_i))^2}{n}} \tag{1}$$

where T_D and T_R = temperatures obtained from the detailed and reduced-order models, respectively; $t_i = i$th time sample; and n = total number of time samples over the heatings period. The RMS temperature deviation was evaluated for temperature histories from the middle surface of the thick part of the slab, where the largest discrepancy was observed in Fig. 6.

First, in Section 3.1 the optimal value of c_p'/c_p was evaluated for the baseline slab configuration (Fig. 4). Then, in Section 3.2, the influence of the slab geometry on the optimal value of c_p'/c_p was investigated. Finally, Section 3.3 presents recommended values of c_p'/c_p to use for various slab dimensions.

Optimization of Specific Heat for Baseline Slab Configuration

Fig. 6 shows a comparison of temperature histories from the detailed model and from reduced-order models with different ratios of specific heat for the concrete in the rib. Layer-averaged temperature histories from the middle surface of the thick portion of the

J. Struct. Eng., 2020, 146(6): 04020080

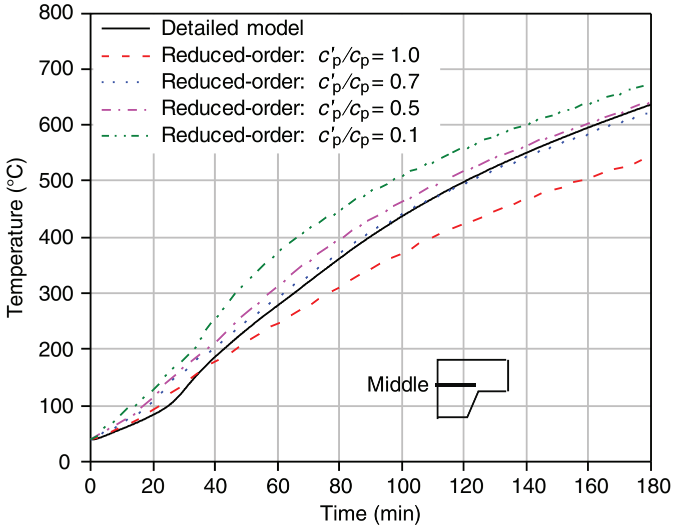

Fig. 6. (Color) Layer-averaged temperature histories (middle surface of thick portion of slab) from the detailed model and from reduced-order models with different specific heat ratios for concrete in the rib.

slab are presented, and corresponding values of the RMS temperature deviation from Eq. (1) are presented in Fig. 7. This figure shows that a specific heat ratio of $c_p'/c_p = 0.7$ yielded the minimum RMS temperature deviation of $T_{\mathrm{RMSD}} = 14$°C, and inspection of Fig. 6 confirms that this ratio produced the best agreement with the temperature history from the detailed model. Fig. 8 shows a comparison of temperature histories from the detailed model with those from the reduced-order model for the optimal specific heat ratio of $c_p'/c_p = 0.7$ at all of the locations shown previously in Fig. 6. Comparison of Fig. 8 with Fig. 3 shows that the optimization resulted in considerably improved agreement at the middle surface of the thick portion of the slab, with no appreciable change in the discrepancies at other locations, including the thin portion of the slab. For the optimal specific heat ratio of $c_p'/c_p = 0.7$ (Fig. 8),

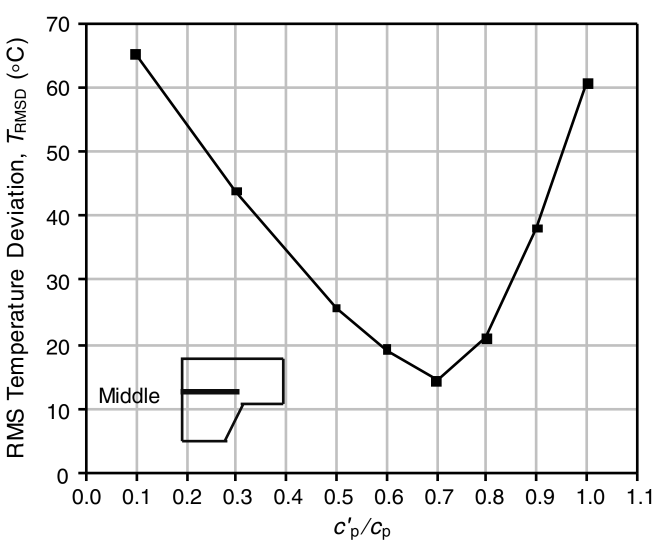

Fig. 7. RMS deviation from the detailed model of layer-averaged temperature histories (middle surface of thick portion of slab) from reduced-order models with different specific heat ratios for concrete in the rib.

the computed temperatures from the detailed and reduced-order models after 180 min of heating differed by 3% or less at all locations.

Influence of Slab Geometry on Optimal Value of Specific Heat

For the baseline slab geometry of Fig. 4, scaling the specific heat of concrete in the rib to $c_p' = 0.7c_p$ was found to minimize the RMS deviation between temperature histories from the detailed and reduced-order models. This section presents a parametric study on the influence of the slab geometry on the optimal ratio for the artificial specific heat, c_p'/c_p. Of particular interest in this study is the temperature history at the top of the rib (middle surface of the thick portion of the slab in Fig. 6). The discrepancies between the detailed and reduced-order models were consistently largest at this location, as a result of missing heat input through the web of the decking, which cannot be directly modeled within the layered shell formulation. Parametric studies by the authors (Jiang et al. 2017) found that the top of the rib (point C) was most sensitive to variations in the height of the rib, h_2, and the width at the top of the rib, l_1, which governs the angle of the web, α (Fig. 4). Variations in the other slab dimensions had a relatively minor influence on the temperature at the top of the rib. For this reason, a parametric study was conducted to investigate the influence of h_2 and l_1 on the optimal ratio of the artificial specific heat for concrete in the rib, c_p'/c_p. In this parametric study, h_2 and l_1 were varied independently, while the other slab dimensions were not varied from the baseline values.

In addition to the baseline rib height of $h_2 = 75$ mm, for which results were previously presented in Figs. 7 and 8, two additional rib heights of $h_2 = 50$ mm and $h_2 = 100$ mm were selected for the parametric study. For these two rib heights, Fig. 9 shows a comparison of temperature histories from detailed models and from reduced-order models with different ratios of specific heat for the concrete in the rib. Layer-averaged temperature histories from the middle surface of the thick portion of the slab are presented in Fig. 9, and corresponding values of the RMS temperature deviation [from Eq. (1)] are presented in Fig. 10.

For $h_2 = 50$ mm, Fig. 9(a) shows that a specific heat ratio of $c_p'/c_p = 0.3$ yielded the minimum RMS temperature deviation of $T_{\mathrm{RMSD}} = 16$°C. For $h_2 = 100$ mm, Fig. 9(b) shows that a specific heat ratio of $c_p'/c_p = 1.5$ yielded the minimum RMS temperature deviation of $T_{\mathrm{RMSD}} = 36$°C. For the baseline rib height of $h_2 = 75$ mm, an optimal value of $c_p'/c_p = 0.7$ was previously identified from Fig. 7. It is helpful to present these results in terms of the ratio of the concrete topping height to the rib height, h_1/h_2, where $h_1 = 85$ mm in all cases. Optimal specific heat ratios of $c_{\mathrm{p}}'/c_{\mathrm{p}} = 0.3$, 0.7, and 1.5 then correspond to height ratios of $h_1/h_2 = 1.70$, 1.13, and 0.85, respectively. These results indicate that when $h_1 > h_2$, the heat input through the web of the decking is underestimated. This corresponds to the case in which the dummy material spans less than half of the total slab height (Fig. 3). Artificially reducing the specific heat of concrete in the rib then helps to increase the flow of heat energy from the dummy material (in Shell B) into the adjoining layers of the rib (in Shell A), thus increasing the temperature at the top of the rib. Conversely, when $h_1 < h_2$, the heat input through the web of the decking is overestimated. This corresponds to the case in which the dummy material spans more than half of the total slab height. Artificially increasing the specific heat of concrete in the rib then helps to reduce the flow of heat energy from the dummy material into the adjoining layers of the rib, thus reducing the temperature at the top of the rib. The ratio h_1/h_2, which is inversely proportional to the height of the dummy

J. Struct. Eng., 2020, 146(6): 04020080

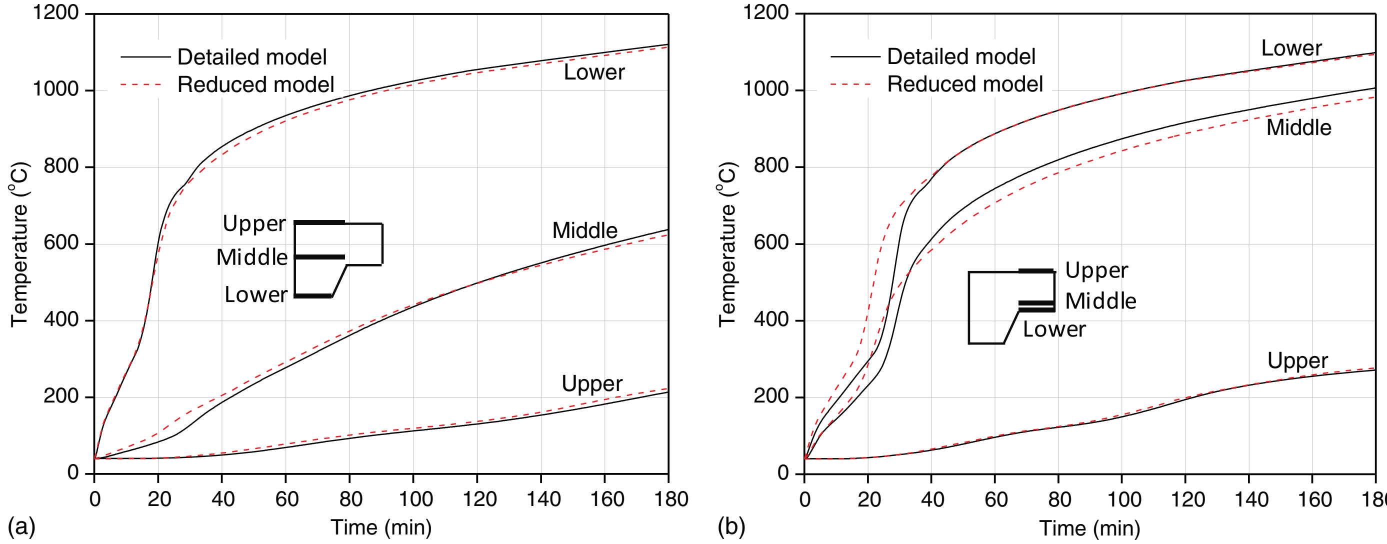

Fig. 8. (Color) Layer-averaged temperature histories from the detailed model and reduced-order model with optimal specific heat ratio of $c'_p/c_p = 0.7$: (a) thick portion of slab; and (b) thin portion of slab.

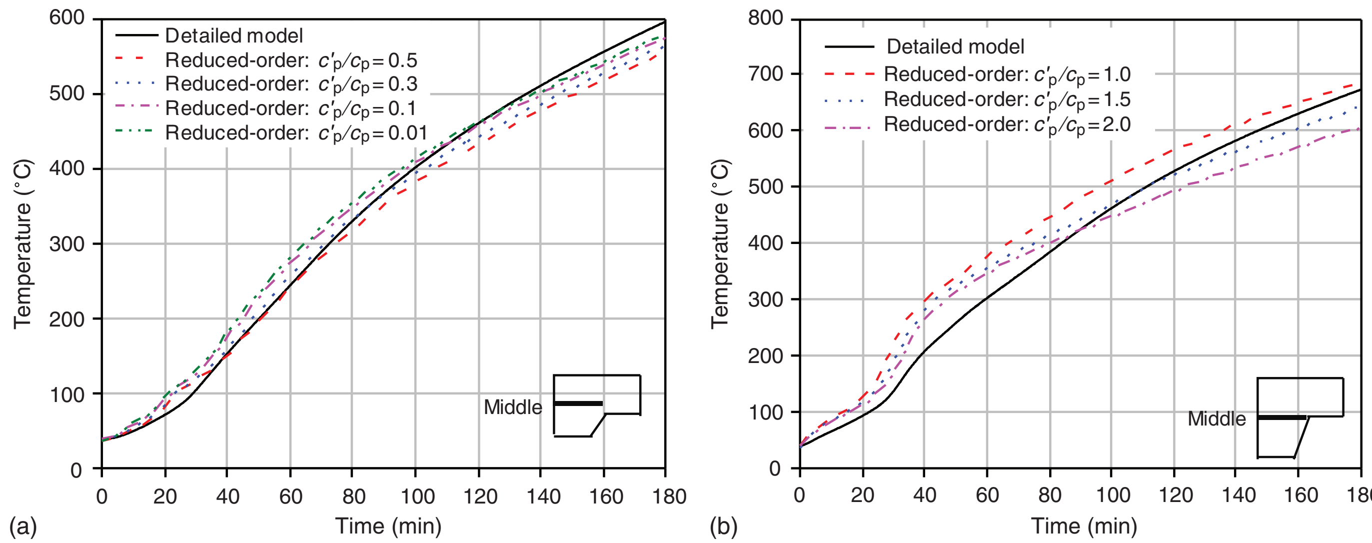

Fig. 9. (Color) Layer-averaged temperature histories (middle surface of thick portion of slab) from the detailed model and from reduced-order models with different specific heat ratios for concrete in the rib: (a) $h_2 = 50$ mm; and (b) $h_2 = 100$ mm.

material, is thus seen to be an important factor influencing the optimal ratio for the artificial specific heat of concrete in the rib.

In addition to the baseline value of $l_1 = 184$ mm for the width at the top of the rib (web angle of $\alpha = 67°$), two additional values of $l_1 = 130$ mm ($\alpha = 86°$) and $l_1 = 250$ mm ($\alpha = 50°$) were selected for the parametric study. For these two values, Fig. 11 shows a comparison of temperature histories from detailed models and from reduced-order models with different ratios of specific heat for the concrete in the rib. Corresponding values of the RMS temperature deviation for the temperature histories in Fig. 11 are presented in Fig. 12. Results for the baseline geometry were previously presented in Figs. 7 and 8. These results show that for $l_1 = 130$, 184, and 250 mm, minimum values of $T_{\mathrm{RMSD}} = 22$°C, 10°C, and 14°C were obtained corresponding to optimal specific heat ratios of $c'_p/c_p = 0.5$, 0.7, and 0.7, respectively. For $l_1 = 130$ mm, it is noted that the RMS temperature deviation is almost equivalent for $c'_p/c_p = 0.5$ and for $c'_p/c_p = 0.7$, and thus a value $c'_p/c_p = 0.7$ is nearly optimal for all values of l_1. The optimal value of c'_p/c_p is thus seen to be much less sensitive to variations in l_1 than to variations in h_1/h_2. Recommended values of c'_p/c_p for varying slab geometry are presented in the following section.

Recommended Values of Specific Heat for Concrete in the Rib

The parametric study in the previous section demonstrated that modifying the specific heat of concrete in the rib could effectively reduce the discrepancies resulting from the missing heat input through the web of the decking, which can only be approximately modeled within the reduced-order, layered-shell approach.

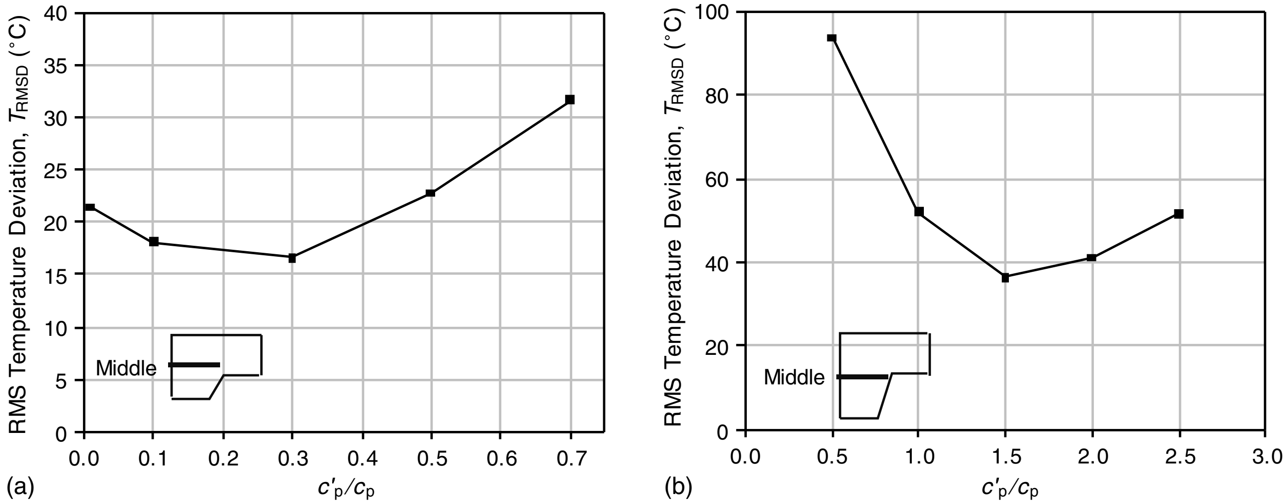

Fig. 10. RMS deviation from the detailed model of layer-averaged temperature histories (middle surface of thick portion of slab) from reduced-order models with different specific heat ratios for concrete in the rib: (a) $h_2 = 50$ mm; and (b) $h_2 = 100$ mm.

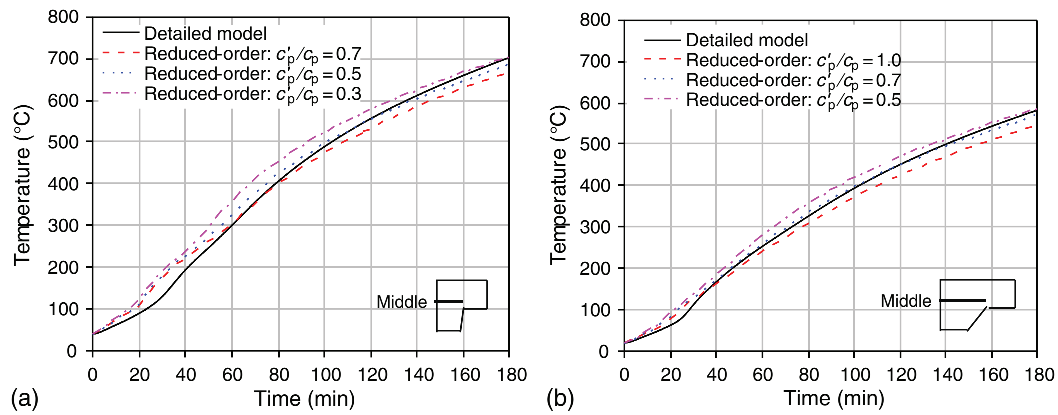

Fig. 11. (Color) Layer-averaged temperature histories (middle surface of thick portion of slab) from the detailed model and from reduced-order models with different specific heat ratios for concrete in the rib: (a) $l_1 = 130$ mm; and (b) $l_1 = 250$ mm.

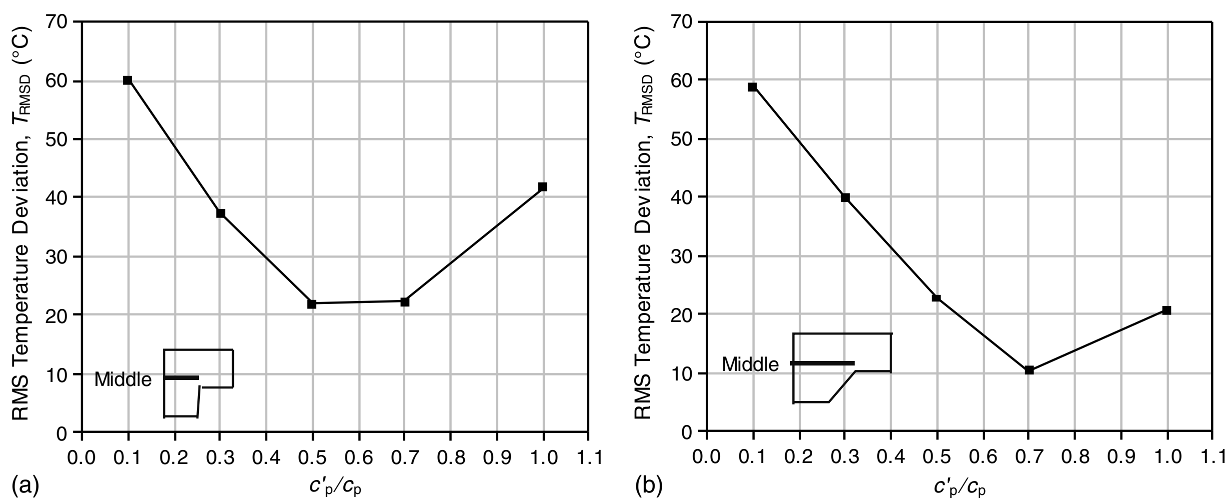

Fig. 12. RMS deviation from the detailed model of layer-averaged temperature histories (middle surface of thick portion of slab) from reduced-order models with different specific heat ratios for concrete in the rib: (a) $l_1 = 130$ mm; and (b) $l_1 = 250$ mm.

Table 1. Optimal and recommended specific heat ratios for concrete in the rib for different slab dimensions

Slab dimensions			Optimal values		Recommended values	
h_2 (mm)	l_1 (mm)	h_1/h_2	c'_p/c_p	T_{RMSD} (°C)	c'_p/c_p	T_{RMSD} (°C)
50	184	1.70	0.3	17	0.5	23
75	184	1.13	0.7	14	0.67	25
100	184	0.85	1.5	36	1.0	52
75	130	1.13	0.5	22	0.67	22
75	184	1.13	0.7	14	0.67	25
75	250	1.13	0.7	10	0.67	23

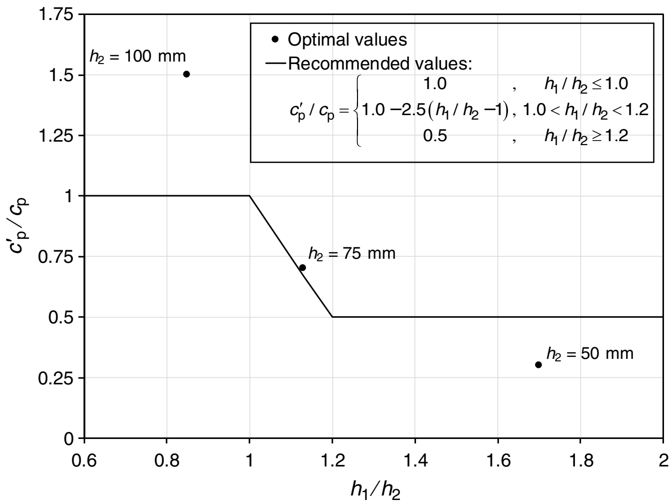

Fig. 13. Recommended specific heat of concrete in the rib as a function of h_1/h_2.

Heat transfer from the dummy material in Shell B into the adjacent layers of the rib in Shell A was significantly influenced by the specific heat in the rib, which allowed for improved accuracy through the optimization of this value. Table 1 summarizes the results of this parametric study, presenting optimal values of the specific heat ratio c'_p/c_p and corresponding minimum values of the RMS temperature deviation for variations of the two slab dimensions, h_2 and l_1. The optimal value of the specific heat ratio was found to be insensitive to variations in l_1, but quite sensitive to variations in h_2, which is conveniently represented through the ratio h_1/h_2. For $h_1/h_2 > 1$, optimal values of the specific heat ratio c'_p/c_p were less than unity, while for $h_1/h_2 < 1$, the optimal value of c'_p/c_p was greater than unity.

Based on the results of the parametric study presented in Table 1, Fig. 13 presents a practical recommendation for estimating the specific heat ratio c'_p/c_p as a function of h_1/h_2, in which c'_p/c_p is reduced linearly from a value of 1.0 for $h_1/h_2 = 1$ to a value of 0.5 for $h_1/h_2 = 1.2$. The slope of this linear reduction is based on the slope between the optimal values of c'_p/c_p for $h_2 = 75$ mm and $h_2 = 100$ mm (shown as solid circles in Fig. 13). The recommended value of c'_p/c_p has an upper limit of 1.0 for $h_1/h_2 < 1$ because Fig. 9(b) shows that values of c'_p/c_p exceeding 1.0 can result in the underestimation of temperatures in the later stages of heating, which is not conservative, while Fig. 10(b) shows that increasing c'_p/c_p beyond 1.0 produces only marginal reductions in the RMS temperature deviation. Artificially increasing the specific heat of concrete in the rib is thus not recommended. Similarly, the recommended value of c'_p/c_p has a lower limit of 0.5 for $h_1/h_2 > 1.2$, because Fig. 10(a) shows that reducing c'_p/c_p below 0.5 produces only marginal reductions in the RMS temperature deviation. Note that these recommended values are applicable for composite slabs with trapezoidal galvanized steel decking within the range of dimensions indicated in Table 1.

Fig. 14 shows a comparison of temperature histories from detailed models and from reduced-order models using the recommended values of c'_p/c_p from Fig. 13 for the three values of h_2 and the three values of l_1 considered in the parametric study of Section 3.2. The recommended values of c'_p/c_p used in these analyses are listed in Table 1 (column 6) along with the resulting RMS deviations between temperature histories from the detailed and reduced-order models in Fig. 14. The RMS temperature deviations are slightly larger than those for the optimal value of c'_p/c_p, but in all cases the discrepancy between the detailed and reduced models at the end of the analysis was less than 10%.

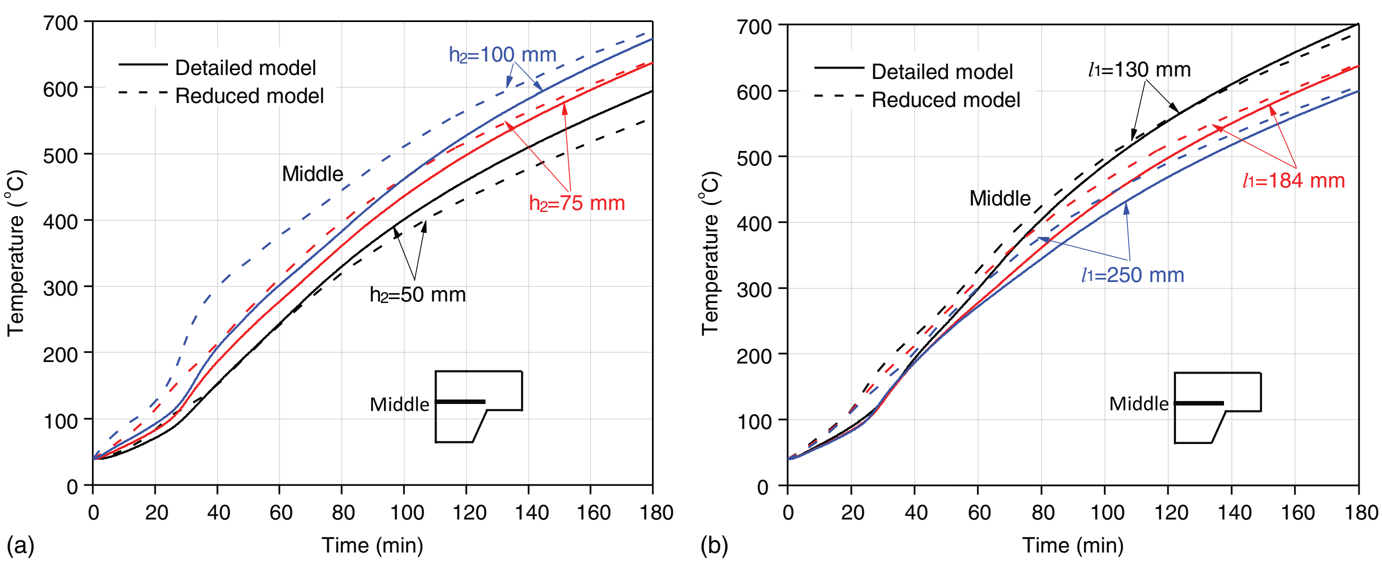

Fig. 14. (Color) Comparison of layer-averaged temperatures at the middle surface of the thick portion of the slab from detailed models and from reduced-order models with recommended values of specific heat in the rib: (a) for different values of h_2; and (b) for different values of l_1.

J. Struct. Eng., 2020, 146(6): 04020080

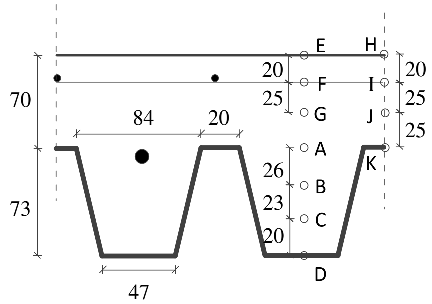

Fig. 15. Geometry of TNO tested slab (dimensions in millimeters). (Data from Hamerlinck et al. 1990.)

Validation of Reduced-Order Modeling Approach

This paper presents validation of the proposed reduced-order modeling approach against experiments under standard fire conditions. Ongoing work is evaluating the applicability of this approach for realistic fire conditions through comparison with full-scale experiments on composite beams.

TNO Test

A standard fire test per ISO 834 (ISO 2014) on a simply supported one-way concrete slab [Test 2 from Hamerlinck et al. (1990)] was selected to validate the proposed reduced-order modeling approach. Fig. 15 shows the configuration of the tested slab. The slab had six ribs and used Prins PSV73 (Amsterdam, Netherlands) steel decking and normal-weight concrete with a measured moisture content of 3.4%. Heat transfer parameters reported by Hamerlinck et al. (1990) were used in the modeling, as summarized in the following. The convective heat transfer coefficient for the lower flange of the steel decking was taken as $25\ \mathrm{W/(m^2 \cdot K)}$, and a lower value of $15\ \mathrm{W/(m^2 \cdot K)}$ was used for the web and upper flange of the decking to consider the shielding effect of ribs. A convective heat transfer coefficient of $8\ \mathrm{W/(m^2 \cdot K)}$ and an emissivity of 0.78 were used for the unexposed top concrete surface. View factors for the upper flange and the web of the steel decking were 0.3 and 0.6, respectively, and a view factor of 1.0 was used for the lower flange of the steel decking and the unexposed top concrete surface.

Fig. 16 presents a comparison of the measured temperature histories from the TNO slab test with the computed temperatures from the detailed and reduced-order models. For consistency with the experimental measurements, point temperatures rather than layer-averaged temperatures are presented from the numerical models (i.e., nodal temperatures, rather than element temperatures, are presented from the reduced-order model). The TNO slab had a height ratio of $h_1/h_2 = 0.96$, for which Fig. 13 recommends a specific heat ratio of $c_p'/c_p = 1.0$, and therefore, no modification of the specific heat of concrete in the rib was used in the reduced-order model of the TNO test. For comparison with the computed results, the measured temperature at point M (midheight of the thick portion of the slab) was obtained by interpolation of measured temperatures at adjacent points (points A and G in Fig. 15).

Table 2 presents RMS deviations between the measured and computed temperature histories shown in Fig. 16 [calculated from Eq. (1)], as well as percent deviations at the end of the test. The largest discrepancies were at point K, where the RMS temperature deviations were 42°C and 73°C for the detailed and reduced-order models, respectively. At all other locations, the RMS temperature deviations were less than 30°C. The largest percent deviations at the end of the test were +14% and +17% for the detailed and reduced-order models, at points H and E, respectively.

BRANZ Test

The reduced-order modeling approach was also validated against a two-way composite slab tested in the Building Research Association of New Zealand (BRANZ) furnace (Lim 2003). The configuration of the slab's cross section is shown in Fig. 17. The tested slab was 3.15-m wide and 4.15-m long, and was exposed to the ISO 834 fire for 3 h. The Dimond Hibond steel decking had a thickness of 0.75 mm and a total depth of 130 mm. Normal-weight concrete was used with siliceous aggregates. The same thermal loading and boundary conditions as the TNO test were used, expect for the view factors taken for the upper flange and web as 0.8 and 0.63, respectively.

Fig. 18 shows a comparison of the measured temperature histories from the BRANZ slab test (Lim 2003) with the computed

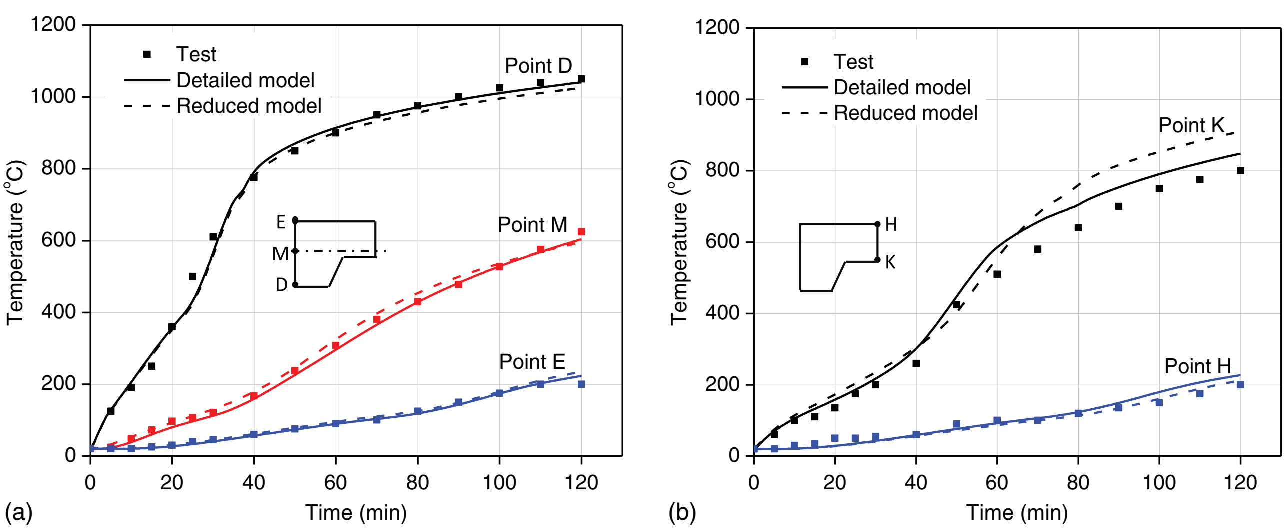

Fig. 16. (Color) Comparison of measured temperatures from TNO test (Hamerlinck et al. 1990) with computed temperatures from detailed and reduced-order models: (a) thick portion of slab; and (b) thin portion of slab.

Table 2. Root-mean-square and percent deviations between measured and computed temperatures at the five locations shown in Fig. 16 for the TNO test

	RMS temperature deviation, T_{RMSD}		Percent deviation[a] at end of test	
Location	Detailed model (°C)	Reduced-order model (°C)	Detailed model (%)	Reduced-order model (%)
Point D	25	30	−1	−2
Point M	11	14	−3	−5
Point E	7	10	+11	+17
Point K	42	73	+6	+14
Point H	17	12	+14	+6

Source: Data from Hamerlinck et al. (1990).
[a]Positive deviations indicate that the model was conservative.

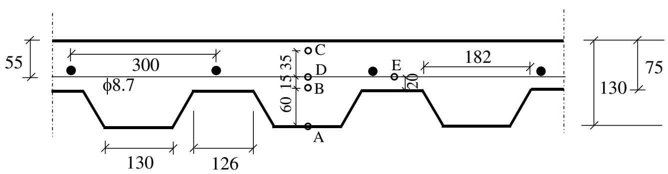

Fig. 17. Geometry of BRANZ tested slab (dimensions in millimeters). (Data from Lim 2003.)

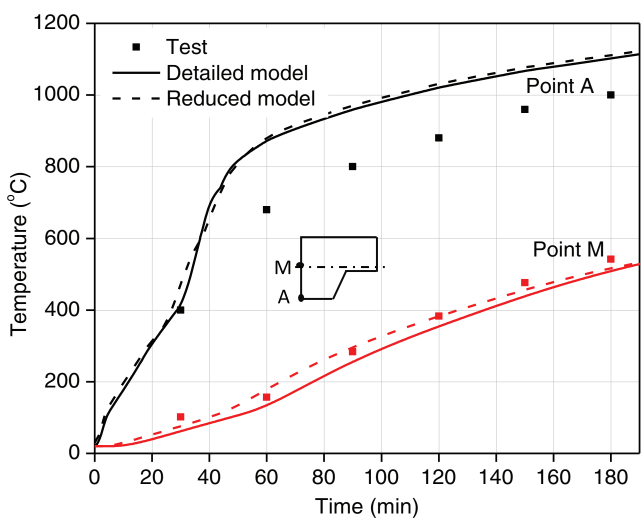

Fig. 18. (Color) Comparison of measured temperatures from BRANZ test (Lim 2003) with computed temperatures from the detailed and reduced-order models.

Table 3. Root-mean-square and percent deviations between the measured and computed temperatures at the two locations shown in Fig. 18 for the BRANZ test

	RMS temperature deviation, T_{RMSD}		Percent deviation[a] at end of test	
Location	Detailed model (°C)	Reduced-order model (°C)	Detailed model (%)	Reduced-order model (%)
Point A	131	142	+10	+11
Point M	32	20	−6	−5

Source: Data from Lim (2003).
[a]Positive deviations indicate that the model was conservative.

temperatures from the detailed and reduced-order models. The BRANZ slab had a height ratio of $h_1/h_2 = 1.4$, for which Fig. 13 recommends a specific heat ratio of $c'_p/c_p = 0.5$, and therefore, the specific heat of concrete in the rib was reduced to half of the value used elsewhere in the slab. The computed temperatures at point A (for both the detailed and reduced-order models) were higher than the measured results as a consequence of the debonding of the steel decking from the concrete that occurred during the test. Table 3 presents RMS deviations between the measured and computed temperature histories shown in Fig. 18 [calculated from Eq. (1)], as well as percent deviations at the end of the test. Because of the debonding that occurred, the largest discrepancies were at point A, where both the detailed and reduced-order models had RMS temperature deviations of approximately 140°C and percent deviations of approximately +10% at the end of the test. Better agreement was observed at point M, where the RMS temperature deviations were 32°C or less and the percent deviations at the end of the test were −6% or less for both the detailed and reduced-order models.

Summary and Conclusions

This paper presented a reduced-order modeling approach that used a layered composite shell formulation for heat transfer analysis of composite slabs. This approach can be readily extended to thermal/structural analysis using the same modeling approach. The geometry of composite slabs was captured by using alternating strips of shell elements to represent the thick and thin portions of the slab, with a linear reduction in the density of concrete with depth in the rib to account for the tapered profile of the ribs. Shell elements representing the thin portions of the slab incorporated a dummy material with low specific heat and high thermal conductivity to represent the voids between the ribs, allowing the thick and thin portions of the slab to be modeled using shell elements with the same thickness. The reduced-order modeling approach was calibrated against detailed models of composite slabs with lightweight concrete and validated against experimental results for composite slabs with normal-weight concrete, thus demonstrating the applicability of the proposed approach to both types of concrete.

Adequately accounting for heat input through the web was found to be the greatest challenge in accurately modeling heat transfer using the reduced-order modeling approach, and artificially reducing the specific heat of concrete in the rib was found to be an effective method to achieve this. The modification factor for the specific heat in the rib, c'_p/c_p, was recommended as 0.5 for slabs with $h_1/h_2 > 1.2$ and as 1.0 for slabs with $h_1/h_2 < 1.0$, with a linear interpolation between these values for h_1/h_2 between 1.0 and 1.2. Comparison of experimentally measured temperature histories with those computed from the reduced-order model showed that the largest root-mean-square temperature deviation (excluding a location where debonding of the decking was known to have influenced the temperature measurement) was 73°C, with a maximum deviation of 17% for the temperature at any location at the end of the test.

Data Availability Statement

Some or all data, models, or code that support the findings of this study are available from the corresponding author upon reasonable request.

Disclaimer

Certain commercial entities, equipment, products, or materials are identified in this document in order to describe a procedure or concept adequately. Such identification is not intended to imply recommendation, endorsement, or implication that the entities, products, materials, or equipment are necessarily the best available for the purpose. The policy of the National Institute of Standards and Technology is to include statements of uncertainty with all NIST measurements. In this document, however, measurements of authors outside of NIST are presented, for which uncertainties were not reported and are unknown.

References

CEN (European Committee for Standardization). 2005. *Eurocode 4: Design of composite steel and concrete structures: Part 1.1: General rules, Structural fire design*, EN 1994-1-2. Brussels, Belgium: CEN.

Elghazouli, A. Y., and B. A. Izzuddin. 2000. "Response of idealised composite beam-slab systems under fire conditions." *J. Constr. Steel Res.* 56 (3): 199–224. https://doi.org/10.1016/S0143-974X(00)00006-7.

Guo, S. 2012. "Experimental and numerical study on restrained composite slab during heating and cooling." *J. Constr. Steel Res.* 69 (1): 95–105. https://doi.org/10.1016/j.jcsr.2011.08.009.

Hamerlinck, R., L. Twilt, and J. Stark. 1990. "A numerical model for fire-exposed composite steel/concrete slabs." In *Proc., 10th Int. Specialty Conf. on Cold-formed Steel Structures*, 115–130. Columbia, MO: Univ. of Missouri.

Huang, Z., I. W. Burgess, and R. J. Plank. 2000. "Effective stiffness modelling of composite concrete slabs in fire." *Eng. Struct.* 22 (9): 1133–1144. https://doi.org/10.1016/S0141-0296(99)00062-0.

ISO. 2014. *Fire-resistance tests–Elements of building construction*, ISO 834-11. Geneva: ISO.

Izzuddin, B. A., X. Y. Tao, and A. Y. Elghazouli. 2004. "Realistic modelling of composite and R/C floor slabs under extreme loading—Part I: Analytical method." *J. Struct. Eng.* 130 (12): 1972–1984. https://doi.org/10.1061/(ASCE)0733-9445(2004)130:12(1972).

Jiang J., J. A. Main, F. Sadek, and J. M. Weigand. 2017. *Numerical modeling and analysis of heat transfer in composite slabs with profiled steel decking*. NIST Technical Note 1958. Gaithersburg, MD: National Institute of Standards and Technology.

Jiang, J., J. A. Main, J. M. Weigand, and F. Sadek. 2020. "Reduced-order modeling of composite floor slabs in fire. II: Thermal-structural analysis." *J. Struct. Eng.* 146 (6): 04020081. https://10.1061/(ASCE)ST.1943-541X.0002607.

Kwasniewski, L. 2010. "Nonlinear dynamic simulations of progressive collapse for a multistory building." *Eng. Struct.* 32 (5): 1223–1235. https://doi.org/10.1016/j.engstruct.2009.12.048.

Lamont, S., A. S. Usmani, and M. Gillie. 2004. "Behaviour of a small composite steel frame structure in a "long-cool" and a "short-hot" fire." *Fire Saf. J.* 39 (5): 327–357. https://doi.org/10.1016/j.firesaf.2004.01.002.

Lim L. C. S. 2003. "Membrane action in fire exposed concrete floor systems." Ph.D. dissertation, Dept. of Civil and Natural Resources Engineering, Univ. of Canterbury.

Lim, L. C. S., A. Buchanan, P. Moss, and J. M. Franssen. 2004. "Numerical modelling of two-way reinforced concrete slabs in fire." *Eng. Struct.* 26 (8): 1081–1091. https://doi.org/10.1016/j.engstruct.2004.03.009.

Main, J. A. 2014. "Composite floor systems under column loss: Collapse resistance and tie force requirements." *J. Struct. Eng.* 140 (8): A4014003. https://doi.org/10.1061/(ASCE)ST.1943-541X.0000952.

Pantousa, D., and E. Mistakidis. 2013. "Advanced modelling of composite slabs with thin-walled steel sheeting submitted to fire." *Fire Technol.* 49 (2): 293–327. https://doi.org/10.1007/s10694-012-0265-x.

Sanad, A. M., S. Lamont, A. S. Usmani, and J. M. Rotter. 2000a. "Structural behaviour in a fire compartment under different heating regimes—Part 1 (slab thermal gradients)." *Fire Saf. J.* 35 (2): 99–116. https://doi.org/10.1016/S0379-7112(00)00024-2.

Sanad, A. M., S. Lamont, A. S. Usmani, and J. M. Rotter. 2000b. "Structural behaviour in a fire compartment under different heating regimes—Part 2 (slab mean temperatures)." *Fire Saf. J.* 35 (2): 117–130. https://doi.org/10.1016/S0379-7112(00)00025-4.